Science of the Total Environment 716 (2020) 137108

Contents lists available at ScienceDirect

Science of the Total Environment

journal homepage: www.elsevier.com/locate/scitotenv

Comparative study on Pb^{2+} removal from aqueous solutions using biochars derived from cow manure and its vermicompost

Weiwen Zhang [1], Wenhui Du [1], Feng Wang [1], Huiting Xu, Tonghe Zhao, Hangjun Zhang, Ying Ding, Weiqin Zhu *

Key Laboratory of Hangzhou City for Ecosystem Protection and Restoration, Hangzhou Normal University, Hangzhou 310036, China

HIGHLIGHTS

- Vermicompost (CV) and its biochar have higher pH, ash content and mineral content.
- Vermicompost-derived biochar was more effective to remove Pb^{2+} ions from solution.
- High pH and minerals contribute to CV derived biochar's Pb^{2+} removal efficiency.
- Existing aromatic alcohol/acid also help CV-derived biochar to remove Pb^{2+} ions.

GRAPHICAL ABSTRACT

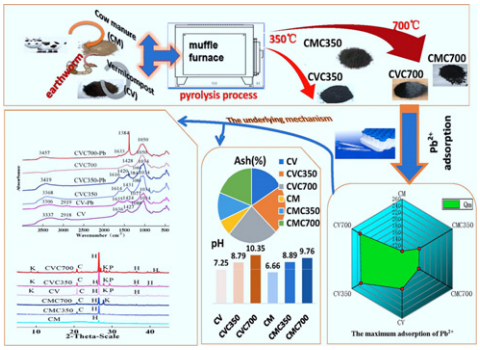

ARTICLE INFO

Article history:
Received 29 July 2019
Received in revised form 1 February 2020
Accepted 2 February 2020
Available online 4 February 2020

Editor: Yong Sik Ok

Keywords:
Cow manure
Vermicompost
Adsorption
Pb^{2+}
Biochar

ABSTRACT

Waste emissions have increased the amount of water and soil contaminated with heavy metals such as Pb. To broaden the methods for the recycling and environmental usage of cow manure (CM) and its vermicompost (CV), CM, CV, and their derived biochars produced by the pyrolysis of CM or CV at 350 and 700 °C were used as adsorbents for Pb^{2+} removal in this batch adsorption experiment to reveal their different Pb^{2+} removal efficiencies and the underlying mechanisms. The batch experiment results revealed that all adsorbents rapidly removed Pb^{2+} within 30 min. A pH between 2.0 and 6.0 positively affected Pb^{2+} removal by CM and its biochar, whereas that by CV and its biochar was only positively affected by pH between 2.0 and 3.0. CV-derived biochar was more effective in the removal of Pb^{2+} than the other absorbents, with the maximum adsorption capacities (Qm) fitted from the Langmuir model reaching approximately 230.0 $mg \cdot g^{-1}$ and the desorption rate (DR) being approximately 0.00–0.02%. Material physiochemical characterization, including X-ray diffraction analysis, showed that high pH, high ash content, rich mineral content, and high mineral contents might have been the main reasons for more effective removal of Pb^{2+} from aqueous solutions by CV-derived biochar. Fourier-transform infrared analysis indicated that surface functional groups such as –OH, C═O, –COO–, and C–O; original and newly produced carbonate; and phosphate in CV also led to more effective Pb^{2+} removal efficiency from aqueous solution via surface functional group binding. Thus, pyrolyzing CVs may be used to produce biochar as a cost-effective adsorbent for heavy metal remediation in soil and water in the future.

Abbreviations: CM, cow manure; CV, vermicompost; XRD, X-ray diffraction; FTIR, Fourier transform infrared; AR, adsorption rate; DR, desorption rate; %yp, yield percentage.

* Corresponding author.
E-mail address: zhwq@hznu.edu.cn (W. Zhu).

[1] These authors contributed equally to this work.

https://doi.org/10.1016/j.scitotenv.2020.137108
0048-9697/

1. Introduction

Waste emissions from mining, agricultural practices, and other industrial activities have increased the amount of water and soil contaminated with heavy metals such as lead (Pb) (Houben et al., 2013). The issue of heavy metals in the environment poses a risk to public health due to their toxicity and non-biodegradability (Inyang et al., 2012). Many conventional methods, including adsorption (Wu et al., 2019; Xue et al., 2019), chemical precipitation (Yang et al., 2019; L. Yang et al., 2019), and electrolysis (Yu et al., 2016), are applied in the field of heavy metal remediation. Adsorption is widely used for heavy metal removal due to the large surface area, microporous nature, low acid-base reactivity, and high availability of adsorbents, such as activated carbon (Yao et al., 2014). Various raw agricultural materials, including crop residues and animal wastes, are commonly used to produce adsorbents for heavy metal removal (H.Y. Wang et al., 2015; Z.Y. Wang et al., 2015; Wnetrzak et al., 2014). In particular, animal waste is used to produce adsorbents due to its high availability and low cost (Zhang and Wu, 2010). Large amounts of compost and vermicompost (CV) are produced by the composting and vermicomposting processes during manure waste disposal and are available to be utilized (Suthar, 2009) and recycled. Our previous reports have shown that both pig manure and its CV can be used as adsorbents for heavy metal removal, with the CV possessing a greater adsorption capacity than the raw material for removing Cu^{2+}, Zn^{2+}, Cd^{2+}, and Pb^{2+} in solution; however, pig manure possesses a high background heavy metal content (Zhu et al., 2008, 2009). The content of Zn, Cu, Cd, and Pb in pig manure has been reported to be as high as 1501 $mg \cdot kg^{-1}$, 980 $mg \cdot kg^{-1}$, 2.4 $mg \cdot kg^{-1}$ and 19.3 $mg \cdot kg^{-1}$, respectively (Peng et al., 2010), while that in CM is only 152 $mg \cdot kg^{-1}$, 46.5 $mg \cdot kg^{-1}$, 1.4 $mg \cdot kg^{-1}$ and 17.8 $mg \cdot kg^{-1}$, respectively (Wang and Li, 2014). In addition, Zhang et al. (2012) reported that the emission of CM was approximately 28.8 $t \cdot year^{-1}$, which is four to nine times that of pig manure (Guo et al., 2013). Moreover, the amount of composts produced from livestock manure far exceeds the need for agricultural usage, and thus, these composts need to be consumed in other ways (Zhang, 2016). Therefore, the exploration of CM and its CV as effective adsorbents for heavy metal removal from soil and water is needed.

Biochar has a large surface area, high stability, and high alkalinity (Chen et al., 2019), and can strongly interact with trace metals (Yin et al., 2016; Ippolito et al., 2017; Alam et al., 2018a, 2018b). Animal waste-derived biochar can help remove heavy metals from wastewater (Cao and Harris, 2010) and is widely used to immobilize heavy metals in contaminated soils (Li et al., 2015). Furthermore, biochars derived from both digested dairy waste and whole sugar beet have been reported to be effective in the removal of Pb^{2+}, Cu^{2+}, Ni^{2+}, and Cd^{2+} (Inyang et al., 2012). Xu et al. (2013a, 2013b) demonstrated that dairy manure biochar is more effective in the removal of Pb^{2+}, Cu^{2+}, Zn^{2+}, and Cd^{2+} from aqueous solutions than rice husk biochar. The raw materials can determine the properties of a biochar (Zhao et al., 2018). As CV is always produced by an earthworm bioreactor with high value-added earthworm products using organic wastes as raw materials, the vermicomposting process can decompose raw organic matter into different forms of humic matter (Zhu et al., 2018); thus, there may be different remediation effects of biochar derived from CM and its CV on heavy metals. However, few studies have compared CM, its CV, and their biochars in terms of heavy metal removal. Thus, this study investigated CM, its CV, and their derived biochars to remove Pb^{2+} from aqueous solutions, aiming specifically (1) to study the adsorption isotherms and adsorption kinetics of these adsorbents and the effect of pH; (2) to investigate the main controlling factors and underlying mechanisms of these adsorbents in the removal of Pb^{2+} ions; and (3) to explore a new method for producing a new cost-effective adsorbent for Pb^{2+} removal with a low background heavy metal content. The novelty of this research is its aim to explore new adsorbents with both easily available raw materials and low heavy metal contents for the remediation of water and soil polluted with heavy metals, as well as to broaden the recycling method of CM or its CV and augment the high value-added products from earthworms during the CV production process.

2. Materials and methods

2.1. Preparation of the adsorbents

CM and its CV were collected from a company in Hangzhou, China. After being air-dried and sieved through a 2 mm mesh, the raw materials were pyrolysed in a laboratory-scale pyrolysis reactor (TNX1100-30 pyrolysis reactor, China) at 350 °C for CMC350 and CVC350 or 700 °C for CMC700 and CVC700 at a heating rate of 10 $°C \cdot min^{-1}$ and nitrogen flow rate of 0.3 $L \cdot min^{-1}$. The produced biochars were then ground and sieved through a 0.15 mm mesh, and the biochar samples from CM were labelled 'CMC350' and 'CMC700', whereas those from CV were labelled 'CVC350' and 'CVC700'. Some CM and CV raw materials were also sieved through a 0.15 mm mesh for experimental adsorption studies.

2.2. Characterization of adsorbents

Sample pH was determined at a 1:20 (w/w) ratio of adsorbent materials to water extract with a pH meter (Mettler Toledo Delta 320, Switzerland). The ash content was analysed according to ASTM specifications (ASTM, 2001). The specific surface area (SBET) was determined using an automatic adsorption instrument (AUTOSORB-1-C, Quantachrome, United States) by adsorbing and desorbing nitrogen at 77 K. The mineral composition was analysed using X-ray diffraction (XRD) (D8 Advance, Bruker, Germany). Fourier transform infrared (FTIR) spectroscopy (Thermo Scientific Nicolet-iS10, United States) was used to characterize the surface functional groups of the adsorption materials. FTIR spectra with wavenumbers from 4000 to 400 cm^{-1} were recorded at 32 scans per point with a resolution of 0.1 cm^{-1}. All chemicals used were of analytical grade, and distilled water was used to prepare all solutions and reagents. All data were obtained from the analysis of three replicates.

2.3. Batch adsorption experiments

The adsorption isotherm study was performed at an initial Pb^{2+} concentration of 100–1000 $mg \cdot L^{-1}$ and a pH of 5.0, and then desorption studies were carried out using 0.01 $mol \cdot L^{-1}$ $NaNO_3$ to desorb the Pb^{2+} ions adsorbed by CM, CV, and their biochars in a shaking orbital incubator (HY-2(A) Vertical Multi-Purpose Vibrator, China) for 24 h. For the pH studies, the initial pH was adjusted to 2.0–6.0 using 0.01 $mol \cdot L^{-1}$ HNO_3 or NaOH, and the initial concentration of Pb^{2+} was set at 700 $mg \cdot L^{-1}$. The adsorption kinetics were studied by varying the time from 1 to 1440 min with an initial Pb^{2+} concentration of 180 $mg \cdot L^{-1}$ and initial pH of 5.0. All batch adsorption experiments were performed at 25 °C in triplicate, and the solid-liquid ratio was set at 4 $g \cdot L^{-1}$ based on a previous report and the practical agricultural application dosage of biochar (Liu et al., 2017). Stock solutions of Pb^{2+} were obtained by dissolving $Pb(NO_3)_2$ in Milli-Q water, and the concentration of Pb^{2+} was determined by flame atomic absorption spectrometry (Shimadzu AA-6800, Japan).

2.4. Calculation method

The yield percentage (yp%) was calculated as the percentage weight of biochar from 100 g CM or CV pyrolysed in a laboratory-scale pyrolysis reactor at 350 °C or 700 °C.

The amount of Pb^{2+} adsorbed (Q_e) was calculated (Lee et al., 2013) as

$$Q_e = V * (C_0 - C_e)/m, \quad (1)$$

and the adsorption rate (AR) was calculated according to

$$AR = (C_0 - C_e)/C_0 * 100\%, \quad (2)$$

where C_0 and C_e are the concentrations of Pb^{2+} ($mg \cdot L^{-1}$) in the initial and equilibrium solutions, respectively. V is the volume of the solution (L), and m is the dry weight of the added adsorption materials (g).

The amount of Pb^{2+} desorbed (Y) was calculated as

$$Y = V * C_e/m, \quad (3)$$

and the desorption rate (DR) was calculated as

$$DR = Y/Q_e * 100\%, \quad (4)$$

where C_e is the concentration of Pb^{2+} in the aqueous phase ($mg \cdot L^{-1}$), V is the volume of the solution (L), and m is the dry weight of the added adsorbents (g).

2.5. Adsorption isotherm model and kinetic model fitting

The data from the adsorption isotherm study were fitted with the Henry, Freundlich, and Langmuir models, expressed mathematically in Eqs. (5), (6), and (7), respectively.

$$Q_e = A + K_h C_e; \quad (5)$$

$$Q_e = K_f C_e^{\,b}; \quad (6)$$

and

$$C_e/Q_e = C_e/Q_m + 1/(K_L * Q_m); \quad (7)$$

where Q_e is the amount of adsorbed Pb^{2+}($mg \cdot g^{-1}$), C_e is the equilibrium concentration ($mg \cdot L^{-1}$) of Pb^{2+}, Q_m is the maximum adsorption capacity ($mg \cdot g^{-1}$) of Pb^{2+}according to the Langmuir model, and A, K_h, K_f, K_L, and b are constants.

The data from the adsorption kinetics study were fitted with three kinetic models, which are expressed mathematically in the following equations:

$$Q_t = a + b * Int, \quad (8)$$

$$Q_t = Q_e * \left(1 - e^{-K_1 t}\right), \quad (9)$$

and

$$1/Q_t = 1/\left(K_2 Q_e^{\,2} * t\right) + 1/Q_e \quad (10)$$

These models are the Elovich, pseudo-first-order, and pseudo-second- order models, respectively, where Q_t is the adsorption amount ($mg \cdot g^{-1}$) of Pb^{2+} at time t (min), Qe is the adsorption amount ($mg \cdot g^{-1}$) of Pb^{2+} at equilibrium, C_e is the concentration ($mg \cdot L^{-1}$) of Pb^{2+} at time t, and K_1, K_2, a, and b are constants.

All parameters were calculated by nonlinear regression analysis using Origin 8.0 (Origin Lab Corporation, Northampton, United States).

3. Results

3.1. Material characterization

3.1.1. Basic physiochemical properties

As shown in Table 1, as the temperature increased from 350 °C to 700 °C, the yp% of biochars derived from CV (CVC350 and CVC700) decreased from 64.86% to 57.2%, and that of biochars derived from CM (CMC350 and CMC700) decreased from 35.3% to 29.94%. The results revealed that a greater yield of biochar could be achieved from CV than from CM at a considerably lower pyrolysis temperature. Similarly, it has been reported that the yield percentage decreased for discarded mushroom-stick biochar with increasing temperature (Wang et al., 2019). However, increased pyrolysis temperature resulted in increased pH in the biochars; the pH was 7.25, 8.79, and 10.35 for CV, CVC350, and CVC700 and was 6.66, 8.89, and 9.76 for CM, CMC350, and CMC700, respectively, demonstrating that CV and its biochar had considerably higher pH values than did CM and its biochar. The ash content, denoted the inorganic matter content of the adsorbents, was 44.75, 59.28, and 67.32% for CV, CVC350, and was CVC700 and 19.57, 34.68, and 53.51% for CM, CMC350, and CMC700, respectively. Thus, there was a considerably higher inorganic matter content in CV than in CM, which may have been caused by the mixed soil and the organic matter being decomposed into inorganic matter during the vermicomposting process since CM is always put in soil for earthworm feeding (Liu, 2004). In addition, increasing the pyrolysis temperature increased the ash content in the biochars derived from both CM and CV. A recent report also showed that the ash content in cow manure biochar increased from 16.49% to 32.84% with increasing temperature (Qin et al., 2019), and Cao and Harris (2010) ascribed the high ash content in manure biochar to the high mineral content in the feedstock. The pyrolysis process, irrespective of pyrolysis temperature, increased the total K, Na, Ca, and Mg content in biochars compared to those in CM and CV. In particular, higher Ca and Mg contents were observed in CV and its biochars than in CM and its biochars, which was consistent with the changes in ash content above because a high ash content may be indicative of minerals such as K, Na, Ca and Mg (Yang et al., 2017). In summary, a higher pH, ash content, and total Ca and Mg content were found in CV and its biochars than in CM and its biochars, which may contribute to the different Pb^{2+} removal efficiencies from solution.

3.1.2. Surface area and pore size

The SBETs and pore sizes of all adsorbents are shown in Table 1. The SBETs of CM and CV were $6.005 m^2 \cdot g^{-1}$ and $4.921 m^2 \cdot g^{-1}$, respectively. The SBET of CVC350 and CVC700 was increased by 3 and 10 times with respect to that of CV, whereas those of CMC350 and CMC700 were increased by 10 and 14 times with respect to that of CM, respectively. Similar reports have also shown that the specific surface area of biochars increased as the pyrolysis temperature increased (Zhang et al., 2019), which can be explained by the fact that the increased temperature helped the decomposition and escape of volatiles, tars and other products, leading to more microporous structures and larger specific surface areas in the biochar (Chen et al., 2019). However, although the average pore diameters were 56.11, 48.39, and 27.01 nm for CV, CVC350, and CVC700 and were 67.64, 24.27, and 24.92 nm for CM, CMC350 and CMC700, respectively, the SBET of CV, CVC350, and CVC700 was consistently lower than that of CM, CM350, and CM700. These results suggest that increasing the pyrolytic temperature can decrease the average pore diameter of biochar derived from CV and may contribute to increased surface area. However, a high pyrolytic temperature primarily led to an increased surface area of biochar from CM but had no contribution

Table 1
Physical and chemical properties of CV, CVC350, and CVC700 and CM, CMC350, and CMC700.

Property	CV	CVC350	CVC700	CM	CMC350	CMC700
yp (%)	–	64.86	57.2	–	35.3	29.94
pH	7.25	8.79	10.35	6.66	8.89	9.76
Ash (%)	44.75	59.28	67.32	19.57	34.68	53.51
K (mg/g)	9.00	15.63	21.10	6.46	16.43	17.23
Na (mg/g)	10.21	13.23	14.91	10.23	11.55	11.53
Ca (mg/g)	31.72	42.84	42.34	8.38	17.09	19.17
Mg (mg/g)	10.44	13.91	15.01	4.07	9.38	9.87
SBET (m^2/g)	4.921	15.80	50.34	6.005	65.38	86.95
Pore size (nm)	56.11	48.39	27.01	67.64	24.27	24.92

Note: yp (%) is the yield percentage of the biochar from their raw materials, S_{BET} is Specific surface area.

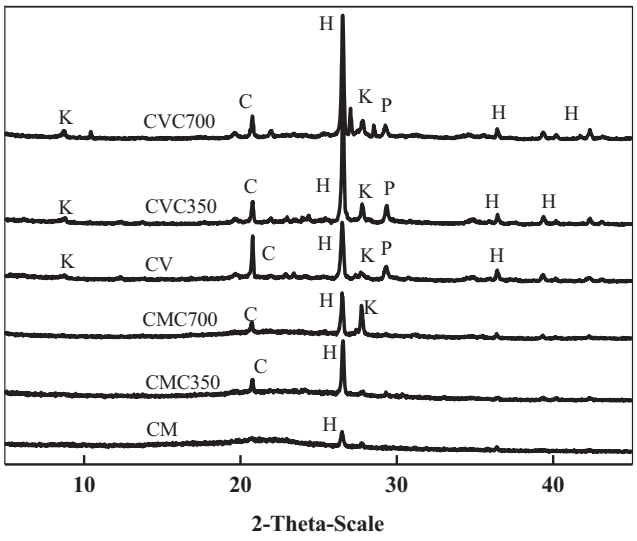

Fig. 1. X-ray diffraction patterns of CV, CVC350, and CVC700 and CM, CMC350, and CMC700 material minerals, with peaks labelled: K, kalicinite ($KHCO_3$); C, quartz (SiO_2); H, halite (NaCl); P, $CaCO_3$.

to the development of its micropores, and smaller micropores did not contribute to the increased surface area of CV compared with that of CM.

3.1.3. XRD analysis

As shown in Fig. 1, based on the characteristic peaks of inorganic components contained in the samples (Kostas et al., 2015; Yuan et al., 2011), sharp peaks in all samples indicated the presence of miscellaneous inorganic components in CM, CV, and their derived biochars. Similar mineral compositions with sharper peaks and higher intensities were observed in CV, CVC350, and CVC700 than in CM, CMC350, and CMC700, including kalicinite ($KHCO_3$, Peak K), quartz (SiO_2, Peak C), halite (NaCl, Peak H), and calcium carbonate ($CaCO_3$, Peak P). With increasing temperature, an increased intensity of peaks H, K, and P and decreased intensity of Peak C were observed in CVC350 and CVC700 compared to those in CV. This result was consistent with the report that increasing the pyrolysis temperature could increase the intensity of some sharp peaks in biochars from dairy manure-derived CV (Yang et al., 2015), suggesting that overall, the considerably higher pyrolysis temperature increased the mineral content, especially the content of kalicinite, halite and calcium carbonate, in the biochars derived from CV. In contrast, only one sharp peak was observed in the spectrum of CM, indicating that halite (NaCl, Peak H) crystalline minerals primarily existed in cow manure. However, similar increasing peak numbers and intensities were observed with increasing pyrolysis temperature, with quartz (SiO_2, Peak C) being observed in both CMC350 and CMC700 and Peak K (kalicinite) being observed in CMC700.Thus, richer minerals and a higher mineral content, especially that of kalicinite, halite and calcium carbonate, occurred in CV and its derived biochar than in CM and its derived biochar. This finding is consistent with the above analysis of the total Ca, Mg and ash contents (Table 1), which may contribute to the difference in the Pb^{2+} removal efficiencies by CM, CV and their biochars.

3.2. Adsorption isotherms

As shown in Fig. 2, the adsorption capacity of Pb^{2+} by all adsorbents increased with an increasing initial Pb^{2+} concentration in solution, and all adsorbents achieved equilibrium except for CVC350 and CVC700, revealing that CVC350 and CVC700 may not have removed the largest amount of Pb^{2+} from solution. As shown in Table 2, the coefficients of determination (R^2) from the Langmuir model for all the adsorbents, ranging from 0.9635 to 0.9991, were far greater than those from both the Henry and Freundlich models, indicating that Pb^{2+} adsorption on all the adsorbents fit the Langmuir model extremely well; similar fitting results have been reported for the adsorption of Pb^{2+} onto sesame straw biochar (Park et al., 2016). As calculated by the Langmuir model, the Qm values of $Pb^{2+}$for CVC350 and CVC700 were close, 227.27 and 230.95 $mg \cdot g^{-1}$, respectively, but both were considerably higher than that of CV, as well as those of other biochars from rice straw, wheat straw and lychee branches reported in recent literatures (Lin et al., 2016). Similarly, the Qm values of Pb^{2+} adsorption on CM were much lower than those of its derived biochars (CMC350 and CMC700). Additionally, the Qm of Pb^{2+} adsorption by CV and its biochars was considerably higher than that of CM and its derived biochars. Yao et al. (2014) reported that K_L from the Freundlich model was related to the affinity between the adsorbate and adsorbent, with a greater K_L signifying greater affinity. As shown in Table 2, the K_L value for the Pb^{2+} adsorption of CVC350 was considerably higher than that of the other materials. Suggesting that CVC350 had a greater affinity for Pb^{2+} in solution. In sum, the Langmuir isotherm model can be used to express Pb^{2+} adsorption on CV, CM and their derived biochars, and biochars from both CV and CM can improve the removal efficiency of Pb^{2+} in solution, with CV derived biochar being the best adsorbent for Pb^{2+} removal.

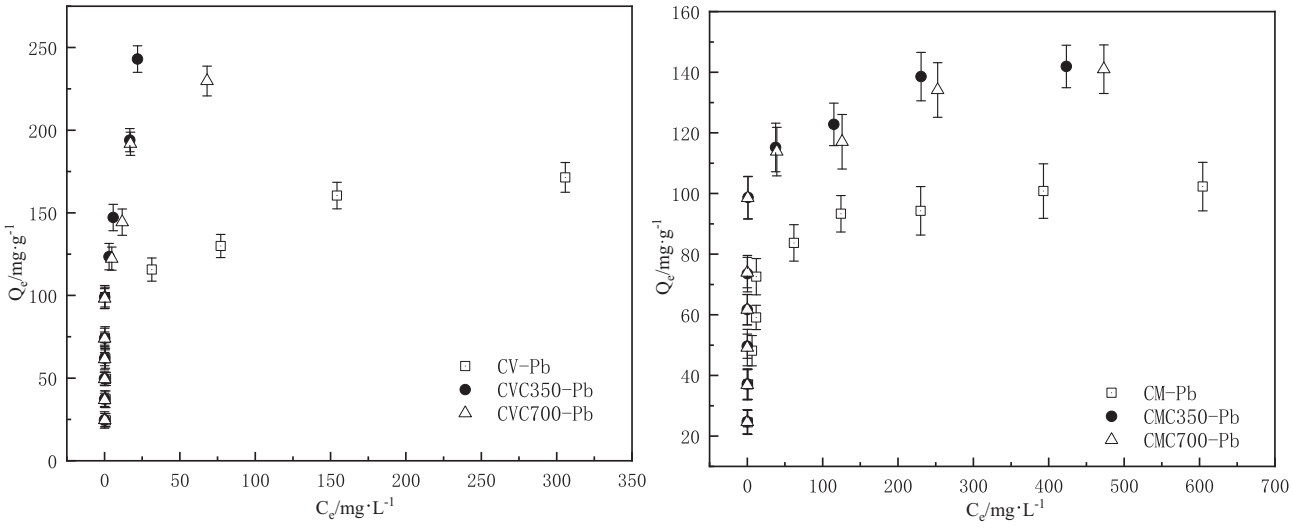

Fig. 2. Adsorption isotherm curve of Pb^{2+} onto CV, CVC350, and CVC700 and CM, CMC350, and CMC700.

Table 2
Some constants of the isotherm equation for Pb^{2+} adsorption on all adsorbents.

Adsorption materials	Henry Qe = A+ K_hCe			Freundlich Qe = K_f*Ce^b			Langmuir Ce/Qe = Ce/Qm + 1/(K_L*Qm)		
	A	K_h	R^2	K_f	b	R^2	Q_m	K_L	R^2
CV	68.49	0.427	0.6320	62.71	0.176	0.7657	170.65	0.167	0.9928
CVC350	65.52	8.323	0.8458	101.44	0.254	0.9116	227.27	1.117	0.9635
CVC700	76.16	2.642	0.6304	90.99	0.222	0.8790	230.95	0.543	0.9864
CM	57.11	0.100	0.4881	39.45	0.161	0.9063	102.77	0.120	0.9991
CMC350	68.62	0.209	0.4872	70.43	0.122	0.8380	141.25	0.333	0.9981
CMC700	67.70	0.195	0.4979	72.23	0.111	0.8266	139.47	0.256	0.9968

3.3. Effect of pH on Pb^{2+} adsorption

pH affects not only the surface charge of the adsorbent but also the ionization and speciation of metal ions in solution. OzCimen and Ersoy-Meriboyu (2010) reported that soluble Pb^{2+}, $PbNO_3^+$, $Pb(NO_3)_2$ and $PbOH^+$ could exist in solution with 0.01 mol·L^{-1} $NaNO_3$ and pH < 7.01; thus, the initial pH was set to values ranging from 2.0 to 6.0 in this experiment. As shown in Fig. 3, pH significantly affected Pb^{2+} adsorption in all adsorbents, and the adsorption capacity of Pb^{2+} by CV and its biochars significantly exceeded that of CM and its biochars throughout the entire pH range. At an initial pH between 2.0 and 3.0, the adsorption capacity of Pb^{2+} by all adsorbent materials dramatically increased. When the initial pH was above 3.0, no increase was observed for Pb^{2+} adsorption by CV, CVC350, and CVC700, whereas a gradual increase was observed for Pb^{2+} adsorption by CM, CMC350, and CMC700, which indicates that pH played a more important role in Pb^{2+} removal by CM and its biochar compared with that by CV and its biochar.

3.4. Adsorption kinetics

As shown in Fig. 4, the adsorption capacity of Pb^{2+} by CM, CV, and their biochars increased rapidly within 30 min before reaching equilibrium. As shown in Table 3, the pseudo-second-order model consistently provided the largest coefficient of determination (R^2) value and best fit to the kinetic adsorption data ($R^2 > 0.9007$) of all biochars. However, the kinetic adsorption of Pb^{2+} by both CV and CM fit the Elovich model better, with considerably higher R^2 values of 0.9134 and 0.8257 for the Elovich model, respectively. It has been reported that pseudo-second-order kinetics can be used to describe the adsorption process dominated by chemical adsorption (Kim et al., 2013). Chang et al. (2016) reported that the Elovich model is based on the assumption that the surface adsorption energy is uniformly distributed during the adsorption process and that the adsorption process is chiefly controlled by surface adsorption. Thus, the kinetic adsorption of Pb^{2+} on CV and CM followed the Elovich kinetic model, controlled by surface adsorption, whereas that on their derived biochars was dominated by chemical adsorption and fit the pseudo-second-order model well.

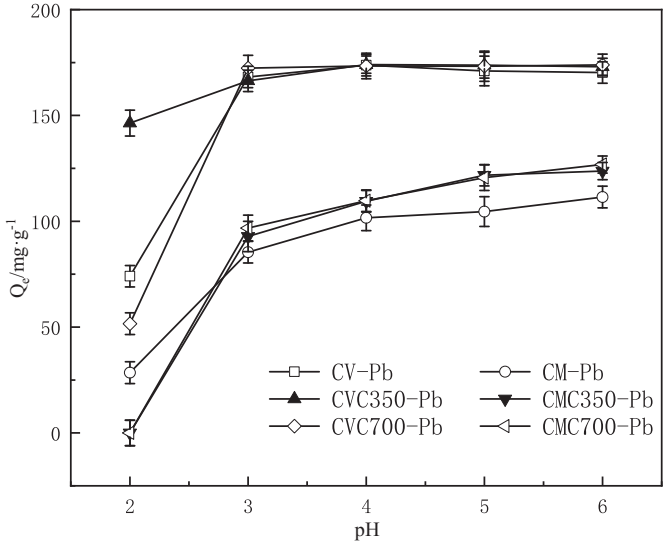

Fig. 3. Effect of initial solution pH on Pb^{2+} adsorption.

3.5. Desorption studies

Desorption studies are important in investigating the binding strength of adsorbates onto an adsorbent and whether heavy metal adsorption is reversible (Camila et al., 2012). As shown in Table 4, with increasing initial Pb^{2+} concentration from 100 to 1000 mg·L^{-1}, the adsorption rate (AR) of Pb^{2+} by CV ranged from 99.91% to 69.43%, which was followed by a desorption rate (DR) ranging from 0.09% to 0.30%, whereas the AR of Pb^{2+} by CVC350 and CVC700 ranged from 99.97% to 93.19%, followed by a DR ranging from 0.00% to 0.02%. Similarly, with increasing initial Pb^{2+} concentration from 100 to 1000 mg·L^{-1}, the AR of Pb^{2+} by CM ranged from 99.22% to 39.57% and was followed by a DR from 0.30% to 6.59%, whereas the AR of Pb^{2+} by CMC350 and CMC700 ranged from 99.97% to 52.70% and was followed by a DR from 0.005% to 0.37%. Thus, CM and CV exhibited considerably lower adsorption rates but much higher desorption rates than their derived biochars, and in particular, CV and its biochars had much higher adsorption rates than CM and its biochars. These findings are of great importance, as they suggest that biochars, particularly vermicompost derived biochars, are considerably more effective in removing and retaining Pb^{2+} at concentrations ranging from100–1000 mg·L^{-1} in aqueous solutions.

3.6. FTIR analysis

As shown in Fig. 5(A) and (B), similar FTIR spectra were observed for CV, CM, and their derived biochars. Based on the results of other studies (Hossain et al., 2011; Wang et al., 2013; Yao et al., 2014; Kostas et al., 2015), broad bands between wavenumbers of 3600 and 3200 cm^{-1} were assigned to hydroxyl (–OH) groups from organic matter, and these peaks decreased rapidly in CVC350, CVC700, CMC350, and CMC700. Wavenumbers from 2920 to 2850 cm^{-1}, indicating the presence of C—H groups in CV and CM, decreased or disappeared abruptly in their derived biochars, suggesting a decrease in nonpolar aliphatic fractions in the biochars from CV and CM (Wang et al., 2013). Aromatic C═O stretching associated with carbonate impurities at wavenumbers ranging from 1620 to 1660 cm^{-1} occurred in CV, CVC350, CM, and CMC350 but disappeared in CVC700 and CMC700. Additionally, the peaks at approximately 1427 cm^{-1} were due to C—O stretching from carbonates (Xu et al., 2013a, 2013b) or primary alcohols and secondary alcohols in CV (Zhu et al., 2012), whereas peaks ranging from 1030 cm^{-1} to 1100 cm^{-1} were assigned to the P—O of PO_4^{3-} or Si—O structures of silicate (Zhu et al., 2012; Xu et al., 2013a, 2013b).

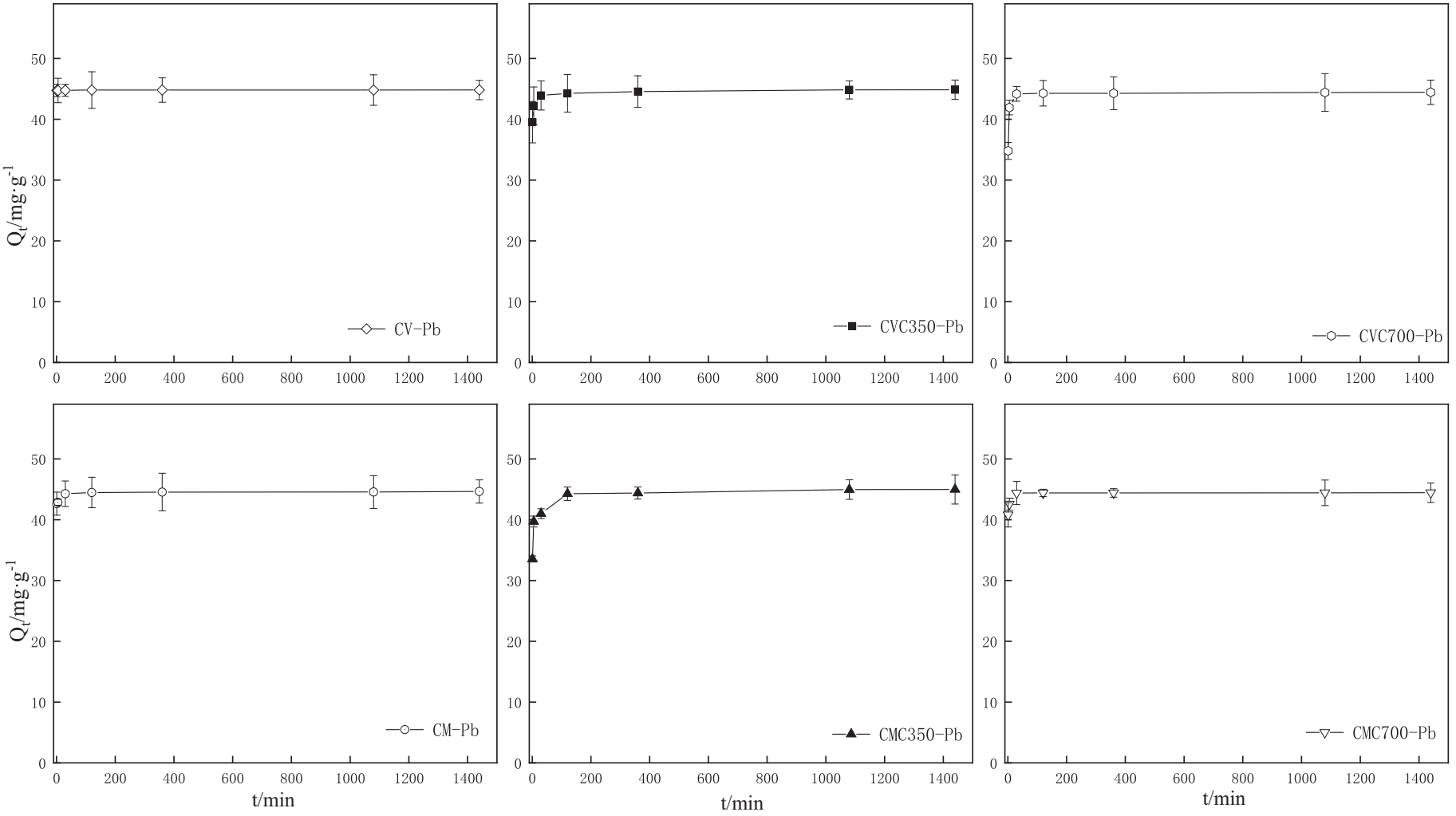

Fig. 4. Kinetics of Pb^{2+} adsorption by CV, CVC350, and CVC700 and CM, CMC350, and CMC700.

Table 3
Parameters of kinetics models for Pb^{2+} adsorption on all adsorbents.

	Elovich $Q_t = a + b\ln t$			Pseudo-first order kinetics $Q_t = Q_e(1- e^{-k1t})$			Pseudo-second order kinetics $1/Q_t = 1/(K_2Q_e^2*t) + 1/Q_e$		
	a	b	R^2	Q_e	K_1	R^2	Q_e	K_2	R^2
CV	44.74	0.011	0.9134	44.79	6.774	0.2195	44.80	1.571	0.4182
CVC350	40.65	0.654	0.8255	44.11	2.265	0.7391	44.37	0.177	0.9173
CVC700	38.14	1.043	0.5891	43.93	1.570	0.9261	44.40	0.081	0.9994
CM	42.77	0.287	0.8257	44.23	3.333	0.3786	44.33	0.503	0.6131
CMC350	35.72	1.425	0.8547	43.23	1.492	0.7087	43.73	0.073	0.9068
CMC700	41.71	0.449	0.7082	44.11	2.590	0.7199	44.29	0.251	0.9007

Note: The bigger is R^2, the better is the model.

Fig. 5(A) shows the FTIR spectra of CV, CVC350, and CVC700, which freely and completely adsorbed Pb^{2+}. The wavenumbers increased from 3337 cm^{-1} and 3368 cm^{-1} to 3306 cm^{-1} and 3419 cm^{-1} after the adsorption of Pb^{2+} by CV and CVC350, respectively, and peaked at 3457 cm^{-1} in CVC700-Pb, indicating the possibility of surface adsorption through complexation with –OH. The bond energies of C═O, –COO–, and C—O were affected by the chemical action generated in the adsorption process, resulting in shifts in the characteristic peak locations from 1636 and 1614 cm^{-1} in CV and CVC350, respectively, to 1662 and 1616 cm^{-1} in CV-Pb and CVC350-Pb, respectively, and an increase in the weak peak at 1633 cm^{-1} in CMC700-Pb. Additionally, the peak at 1427 cm^{-1} in CM shifted to 1424 cm^{-1} in CM-Pb, the peak at 1431 cm^{-1} in CVC350 split into peaks at 1429 and 1384 cm^{-1} in CVC350, and the peak at 1428 cm^{-1} in CVC700 became a sharp peak at 1384 cm^{-1} in CMC700-Pb. These results demonstrate that C═O and C—O from carboxylic acid or their original or newly produced carbonates played an important role in the adsorption of Pb^{2+} by CV and its derived biochar. However, no notable shift was observed for the peak at 2918 cm^{-1} in CV after Pb^{2+} adsorption. Moreover, the peak at 1080 cm^{-1} in CV and CVC350, which disappeared in both CVC700 and CVC700-Pb, corresponding to PO_4^{3-} (Xu et al., 2013a, 2013b), shifted to 1077 cm^{-1} in CV-Pb, whereas no obvious shift was observed in CVC350-Pb, suggesting that the formation of a Pb^{2+} precipitate with phosphate occurred in CV but not in CVC350 and CVC700. Similarly, no shift was observed for the band at approximately 1034 cm^{-1} assigned to Si—O structures in silicate (Zhu et al., 2012) after Pb^{2+} adsorption, revealing that silicate in CV and its derived biochars did not affect the process of Pb^{2+} removal. Therefore, the adsorption of Pb^{2+} on CV and its derived biochar relied on similar functional groups, such as –OH,C═O, –COO– and C—O from aromatic alcohols, aromatic acids and their original or newly produced carbonates, while P—O groups from phosphate may only contribute to the adsorption of Pb^{2+}on CV.

Fig. 5(B) shows the FTIR spectra of CM, CMC350, and CMC700, which freely and completely adsorbed Pb^{2+}. The peak at 3337 cm^{-1} in CM shifted to 3309 cm^{-1} in CM-Pb. Additionally, peaks at 3427 and 3459 cm^{-1} were observed in CMC350-Pb and CMC700-Pb but not in CMC350 and CMC700, indicating the possible complexation of Pb^{2+} with –OH on the surface of CM, CMC350, and CMC700. The peak at 2920 cm^{-1} was observed only in CM and shifted to 2919 cm^{-1} in CM-Pb, revealing that aliphatic fractions could have participated in Pb^{2+} adsorption by CM but not in Pb^{2+} adsorption by CMC350 and CMC700. The shifts of the bands at 1652, 1589, and 1539 cm^{-1} in CM, CMC350, and CMC700 to 1635, 1616, and 1558 cm^{-1} in CM-Pb, CMC350-Pb, and CMC700-Pb, respectively, signified that functional groups from aromatic compounds facilitated the adsorption of Pb^{2+}. Additionally, the emerging peak at 1384 cm^{-1}in only CM-Pb, CMC350-Pb, and CMC700-Pb illustrated a change in the vibration of –COO– from carbonates, suggesting that carbonates played an important role in the adsorption of Pb^{2+}; however, these carbonate groups may not come from the CM or its derived biochar itself, but from the dissolution of CO_2 in the air during the adsorption process. In addition, no shift was observed for the peak at 1100 cm^{-1} in CM and CM-Pb, whereas the peaks at 1100 cm^{-1} in CMC350 and 1104 cm^{-1} in CMC700 shifted to 1104 and 1097 cm^{-1}, respectively, in the FTIR spectra of CMC350-Pb and CMC700-Pb, signifying the participation of Si—O from inorganic compounds in Pb^{2+} adsorption by CMC350 and CMC700. Thus, the adsorption of Pb^{2+} on CM mainly depends on aliphatic alcohols and aromatic alcohols/acids in CM, whereas aromatic alcohols/acids and inorganic silicates may contribute to Pb^{2+} adsorption on CMC350 and CMC700. In addition, carbonate produced during the adsorption process may help improve the Pb^{2+} removal efficiency from aqueous solution.

4. Discussion

4.1. Differences in the physiochemical properties of all adsorbents

Pyrolysis temperature and the raw material are the main factors influencing the biochar yield percentage (Smith et al., 2009; Alam et al., 2018a, 2018b). Our research demonstrated that the yield percentage of biochar from both CM and CV decreased with increasing pyrolysis temperature from 350 to 700 °C, which is consistent with the decreased yield percentage of biochars produced from pecan shell, poultry litter, and switchgrass with increasing pyrolysis temperature (Kostas et al., 2015; Zhang et al., 2019). Thus, a considerably lower pyrolysis temperature should be chosen for biochar production from CM and CV. In addition, the yp% of biochar derived from CV (CVC350 and CVC700) ranged from 64.86% to 57.2%, which is much higher than the 26% yield of maize cob residue biochar (Faloye et al., 2020) and the 51% yield of biochar derived from rice husk (Oladele et al., 2019). Moreover, our study demonstrated that increasing the pyrolysis temperature resulted in an increased pH of biochar from both CM and CV. Shinogi and Kanri (2003) reported that an increased pH of biochar is likely caused by the release of alkali salts from the feedstock during pyrolysis; this process was further demonstrated by the high ash, total Ca, and total Mg contents in the biochars from CM and CV (in Table 1) because the ash

Table 4
The ratio of adsorption and desorption for Pb^{2+} on CV, CVC350, and CVC700 and CM, CMC350, and CMC700.

	CV		CVC350		CVC700		CM		CMC350		CMC700	
	AR(%)	DR(%)	AR(%)	DR(%)	AR(%)	DR(%)	AR(%)	DR(%)	AR(%)	DR(%)	AR(%)	DR(%)
1	99.13	0.30	99.94	0	99.81	0.02	99.22	0.49	99.86	0.08	99.96	0.02
2	99.44	0.18	99.95	0	99.92	0.002	99.22	0.31	99.93	0.02	99.92	0.003
3	99.48	0.13	99.96	0	99.96	0.01	96.79	0.30	99.94	0.01	99.93	0.02
4	99.78	0.24	99.95	0	99.96	0.005	95.23	1.06	99.94	0.04	99.97	0.01
5	99.88	0.22	99.97	0	99.96	0.008	96	0.84	99.94	0.03	99.97	0.02
6	99.91	0.11	99.97	0	99.97	0.008	79.72	1.34	99.73	0.03	99.80	0.02
7	93.71	0.09	99.39	0	99.04	0.006	75.14	2.68	92.45	0.13	92.18	0.005
8	87.14	0.09	99.05	0	98.04	0.011	61.67	4.19	80.85	0.20	79.02	0.02
9	80.71	0.17	97.91	0.007	97.84	0.012	50.89	4.78	71.18	0.27	68.43	0.02
10	69.43	0.24	97.81	0.01	93.19	0.012	39.57	6.59	57.66	0.37	52.70	0.01

Note: From row 1 to row 10, the Pb^{2+} concentration was 100, 150, 200, 250, 300, 400, 500, 600, 800, 1000 $mg \cdot L^{-1}$ respectively; AR is the adsorption rate and DR is the desorption rate.

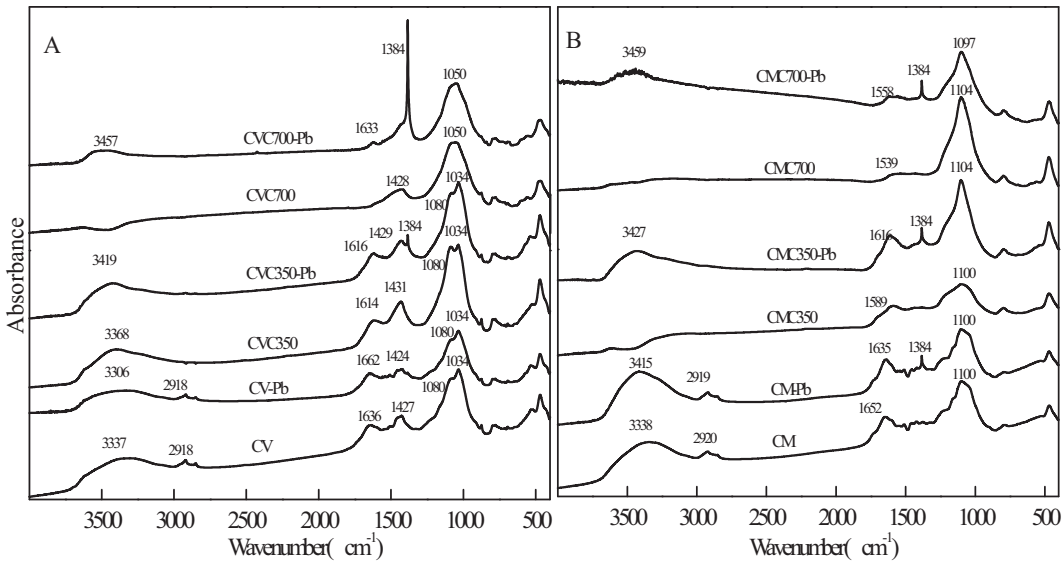

Fig. 5. Stacked FTIR spectra of the adsorbents before and after Pb^{2+} adsorption.

content likely increased the pH. Similarly, XRD analysis showed that CV and its biochars had a higher mineral content, especially kalicinite, halite, and calcium carbonate, than did CM and its derived biochars, which is supported by the report that more abundant mineral species and greater mineral crystallization exist in biochar prepared at higher temperatures (Wei et al., 2019). Zhu et al. (2019) reported that biochar characteristics such as cation exchange capacity (CEC), pH, and ash content account for 53.8% of its adsorption efficiency and that the CEC and pH of biochars are the most important influencing factors among biochar characteristics. High pH may lead to precipitation of heavy metal ions (Sun et al., 2019). Thus, the different pH values of the biochars derived from both CM and CV may be attributed to the increased ash, alkali salts, and mineral contents, especially the increased contents of kalicinite, halite, and calcium carbonate, which may contribute to the removal efficiency of heavy metals from solution.

Our study showed that the pyrolysis process and high temperature increased the surface area of biochars from both CV and CM, which was confirmed by the report that surface area increased at high pyrolytic temperatures (Ahmad et al., 2012). It has also been reported that the development of micropores during carbonization is important for the adsorption of heavy metals because it increases the adsorption surface area (Batool et al., 2019). However, our results suggested that micropores were only observed in the biochars derived from CV, not in the biochars from CM, and a decrease in average pore diameter contributed to an increase in surface area. Thus, differences in pH, mineral content, ash content, and alkali salts, not pore size distribution, may lead to the different removal efficiencies of heavy metals from aqueous solution by CM, CV, and their biochars.

4.2. Different mechanisms for Pb^{2+} removal by all adsorbents

4.2.1. Surface adsorption of Pb^{2+}

Although a high pyrolytic temperature increased the surface area of biochar from both CV and CM, a higher adsorption capacity was only observed for the biochars compared to their raw materials, whereas similar Qm values for Pb^{2+} adsorption were observed between CVC350 and CVC700 and between CMC350 and CMC700; in addition, the Qm value of Pb^{2+} adsorption by CVC350 was nearly twice that of CMC350 irrespective of the obviously lower surface area of CVC350 than that of CMC350, which was in contrast with reports that a higher surface area of biochar enhanced metal sorption (Nigam et al., 2019) and that the improved surface area of modified reed biochar led to enhanced Pb max sorption capacity (Cui et al., 2019). In addition, Agrafioti et al. (2014) reported that sewage sludge biochar has a low surface area but a moderate immobilization capacity for heavy metals. Thus, a surface area-dependent adsorption mechanism may not explain the differences in Pb^{2+} removal among CM, CV, and their biochars.

4.2.2. Co-precipitation of Pb^{2+} with mineral components

There were no obvious changes in the adsorption capacity of Pb^{2+} by CV, CVC350, and CVC700 corresponding to an increase in pH from 3.0–6.0; however, pH still played a role in Pb^{2+} removal by CM and its biochars when the initial pH was above 3.0, which may be correlated with the lower mineral content and pH in CM and its derived biochars than those in CV and its derived biochars (Table 1) because the pH of solution can be affected by alkali ions and minerals released from biochar (Li et al., 2015). Furthermore, considerably richer mineral elements, especially increased contents of kalicinite, halite, and calcium carbonate, were observed in CV, CVC350, and CVC700 in comparison with CM, CMC350, and CMC700, and the adsorption capacity of Pb^{2+} by CV and its biochars was consistently higher than that of CM and its derived biochars. The biochars from both CV and CM increased the removal efficiency of Pb^{2+} in aqueous solution more than their raw materials did (Fig. 2). It has been reported that mineral elements in adsorbents can serve as additional adsorption sites (Gu et al., 2019), and the precipitation reaction between Pb^{2+} and these minerals could be identified as the leading mechanism for Pb^{2+} adsorption on biochars (H.Y. Wang et al., 2015; Z.Y. Wang et al., 2015. Tsai et al. (2019) also indicated that mineral components present in dairy manure-derived biochar may contribute to its high adsorption capacity. Thus, co-precipitation of Pb^{2+} with mineral components in the adsorbent may be one of the major mechanisms controlling the adsorption process. However, there was no notable difference in Q_m between CVC350 and CVC700 or between CMC350 and CMC700, signifying that there may be other components controlling Pb^{2+} adsorption by biochars aside from the mineral content.

4.2.3. The binding of Pb^{2+} with surface functional groups

As shown in Fig. 4, the adsorption capacity of Pb^{2+} by CM, CV, and their derived biochars was lower at an initial pH value of 2.0 than at other pH values, signifying that oxygen-containing functional groups may also participate in the adsorption of Pb^{2+} on the surface of CM, CV, and their derived biochars. It has previously been reported that the pH of the solution can be affected by aromatic compounds and other compounds with functional groups released from biochar (Li et al., 2015) and that oxygen-containing groups may hinder the adsorption of positively charged metal ions on biochar at low pH values (H.Y.

Wang et al., 2015; Z.Y. Wang et al., 2015). Our FTIR analysis demonstrated that functional groups, mainly–OH, C═O, –COO–, and C—O from aromatic compounds, may contribute to Pb^{2+} adsorption by CV and its derived biochars and that adsorption by CM mainly depended on aliphatic alcohols and aromatic compounds. Aromatic alcohols or acids and inorganic silicates may contribute to Pb^{2+} adsorption by CMC350 and CMC700, which is similar to the report that phenolic –OH and aromatic C═O are involved in the adsorption of Cu^{2+}, Zn^{2+}, and Cd^{2+} by dairy manure-derived biochar (Xu et al., 2013a, 2013b). These effects are also supported by reports that surface functional groups, including hydroxyl and carboxylate groups, may interact with heavy metal ions and form surface complexes on adsorbents (Yang et al., 2019; L. Yang et al., 2019; Yu et al., 2018). Chen et al. (2019) reported that increasing the pyrolysis temperature decreased the number of oxygen-containing functional groups, such as hydroxyl and carboxyl groups, which may also help explain why similar Qm values for Pb^{2+} adsorption were observed between CVC350 and CVC700 or between CMC350 and CMC700. However, P—O groups in phosphate, which disappeared in CVC350 and CVC700, may only contribute to Pb^{2+} adsorption by CV, and the original or newly produced carbonate in CV during adsorption may help explain the different removal efficiencies of Pb^{2+} from aqueous solution by CVC350 and CVC700, as well as by CM and its biochars.

5. Conclusion

CM, CV, and their derived biochars rapidly removed Pb^{2+} ions within 30 min. A pH between 2.0 and 6.0 positively affected Pb^{2+} removal by CM and its biochars, whereas that by CV and its biochars was only positively affected by a pH between 2.0 and 3.0. Both CM and CV had considerably lower adsorption rates and higher desorption rates than their corresponding biochars, and Pb^{2+} adsorption by CM, CV, and their derived biochars fit the Langmuir isotherm model well. The biochars, particularly the vermicompost-derived biochars, appeared to be more effective than their raw material in removing and retaining Pb^{2+} from aqueous solutions, with the maximum adsorption capacities of Pb^{2+} reaching approximately 230 $mg \cdot g^{-1}$. Additionally, a greater pH, ash content, and total Ca and Mg contents; richer minerals; and higher mineral contents existed in CV and its biochars than in CM and its biochars. These may be the main underlying factors that increased the removal efficiency of Pb^{2+} from aqueous solution by CV derived biochars via co-precipitation. FTIR analysis showed that surface functional groups such as –OH,C═O, –COO–, and C—O, mainly from aromatic alcohols, aromatic acids, original or newly produced carbonate, and phosphate, led to more effective Pb^{2+} removal efficiency from aqueous solution by CV and its derived biochars. Therefore, using pyrolysed CVs to produce biochars may broaden the options for recycling cow manure and its derived fertilizers. This process can be utilized to produce new cost effective adsorbents for heavy metal remediation in soil and water.

Declaration of competing interest

The authors declare that they have no known competing financial interests or personal relationships that could have appeared to influence the work reported in this paper.

Acknowledgements

The authors wish to thank the Natural Science Foundation of Zhejiang Province (Y17B070004), the Agricultural Scientific Research Projects of Hangzhou City (20180432B08), the National Natural Science Foundation of China (B21207029), the Xinmiao Talents Program of Zhejiang Province (No. 2018R413044), and the Undergraduate Innovation Ability Promotion Project of Hangzhou Normal University (CX2018141, CX2018145) for their partial support of this study.

References

Agrafioti, E., Kalderis, D., Diamadopoulos, E., 2014. Arsenic and chromium removal from water using biochars derived from rice husk, organic solid wastes and sewage sludge. J. Environ. Manag. 133, 314–319.
Ahmad, M., Lee, S.S., Dou, X., 2012. Effects of pyrolysis temperature on soybean stover and peanut shell-derived biochar properties and TCE adsorption in water. Bioresour. Technol. 118, 536–544.
Alam, M.S., Gorman-Lewis, D., Chen, N., Flynn, S.L., Ok, Y.S., Kon-hauser, K.O., Alessi, D.S., 2018a. Thermodynamic analysis of nickel(II) and zinc(II) adsorption to biochar. Environ Sci Technol. 52 (11), 6246–6255.
Alam, M.S., Swaren, L., von Gunten, K., et al., 2018b. Application of surface complexation modeling to trace metals uptake by biochar-amended agricultural soils. Appl. Geochem. 88, 103–112.
ASTM, 2001. Standard Test Method for Chemical Analysis of Wood Charcoal. ASTM International, West Conshohochen, PA.
Batool, S., Idrees, M., Al-Wabel, M.I., Ahmad, M., Hina, K., Ullah, H., Hussain, Q., 2019. Sorption of Cr (III) from aqueous media via naturally functionalized microporous biochar: mechanistic study. Microchem. J. 144, 242–253.
Camila, B.M., Giovana de, F.L., Vanessa, N.A., Nívia, M.M.C., Douglas, C.D., César, R.T.T., 2012. Evaluation of vermicompost as a raw natural adsorbent for adsorption of pesticide methylparathion. Environ. Tech. 2 (33), 167–172.
Cao, X.D., Harris, W., 2010. Properties of dairy-manure-derived biochar pertinent to its potential use in remediation. Bioresour. Technol. 101 (14), 5222–5228.
Chang, C., Wang, S.L., Guo, J.Y., Liu, T.Q., Zhao, Y.Y., 2016. Adsorption kinetics and mechanism of copper ion on biochar with different pyrolysis condition. Acta Sci. Circumst. 36 (7), 2491–2502.
Chen, W.F., Meng, J., Han, X.R., Lan, Y., Zhang, W.M., 2019. Past, present, and future of biochar. Biochar 1, 75–87.
Cui, L., Chen, T., Yin, C., et al., 2019. Mechanism of adsorption of cadmium and Lead ions by iron-activated biochar. BioResources 14 (1), 842–857.
Faloye, O.T., Ajayi, A.E., Alatise, M.O., et al., 2020. Nutrient uptake, maximum yield production, and economic return of maize under deficit irrigation with biochar and inorganic fertiliser amendments. Biochar 2020, 1–14.
Gu, S., Kang, X., Wang, L., Lichtfouse, E., Wang, C., 2019. Clay mineral adsorbents for heavy metal removal from wastewater: a review. Environ. Chem. Lett. 17 (2), 629–654.
Guo, H., Zhao, Y.K., Zhu, C.X., 2013. Research Progress in resource utilization of cattle manure. Environ. Sci. Technol. 36 (5), 68–75.
Hossain, V.S.K., Mustafa, K., Yin, C., 2011. Influence of pyrolysis temperature on production and nutrient properties of wastewater sludge biochar. J. Environ. Manag. 92, 223–228.
Houben, D., Evrard, L., Sonnet, P., 2013. Beneficial effects of biochar application to contaminated soils on the bioavailability of Cd, Pb and Zn and the biomass production of rapeseed (Brassica napus L.). Biomass Bioenergy 57, 196–204.
Inyang, M., Gao, B., Yao, Y., Xue, Y.W., Zimmerman, A.R., Pullammanappallil, P., Cao, X.D., 2012. Removal of heavy metals from aqueous solution by biochars derived from anaerobically digested biomass. Bioresour. Technol. 110, 50–56.
Ippolito, J.A., Berry, C.M., Strawn, D.G., Novak, J.M., Levine, J., Harley, A., 2017. Biochars reduce mineland soil bioavailable metals. J. Environ. Qual. 46, 411–419.
Kim, W.K., Shim, T.Y., Kim, Y.S., et al., 2013. Characterization of cadmium removal from aqueous solution by biochar produced from a giant Miscanthus at different pyrolytic temperatures. Bioresour. Technol. 138, 266–270.
Kostas, K., Dimitra, Z., Ioannis, P., et al., 2015. Assessment of pistachio shell biochar quality and its potential for adsorption of heavy metals. Waste Biomass Valor 6, 805–816.
Lee, Y., Park, J., Ryu, C., Gang, K.S., Yang, W., 2013. Comparison of biochar properties from biomass residues produced by slow pyrolysis at 500°C. Bioresour. Technol. 148, 196–201.
Li, M., Lou, Z., Wang, Y., Liu, Q., Zhang, Y., Zhou, J., Qian, G., 2015. Alkali and alkaline earth metallic (AAEM) species leaching and Cu(II) sorption by biochar. Chemosphere 119, 778–785.
Lin, N., Zhang, H., Jia, Z.Z., et al., 2016. Adsorption of Pb(II)by biochars derived from three types of biomass. Journal of Agro-Environment. Science 35 (5), 992–998.
Liu, D.K., 2004. Effects of earthworm treatment on cow manure [A]. Proceedings of the national symposium on non-point source pollution and integrated control of agriculture [C]. Chinese Society of Agronomy 2.
Liu, Y.X., Huang, B., Zhang, L., 2017. Adsorption of heavy metal Cr^{6+} and Cu^{2+} in aqueous solutions by peanut shell biochar. Science Technology and Engineering 17 (13), 81–85.
Nigam, N., Yadav, V., Khare, P., et al., 2019. Exploring the benefits of biochar over other organic amendments for reducing of metal toxicity in Withania somnifera. Biochar 1 (3), 293–307.
Oladele, S., Adeyemo, A., Adegaiye, A., et al., 2019. Effects of biochar amendment and nitrogen fertilization on soil microbial biomass pools in an Alfisol under rain-fed rice cultivation. Biochar 1 (2), 163–176.
OzCimen, D., Ersoy-Meriboyu, A., 2010. Characterization of biochar and bio-oil samples obtained from carbonization of various biomass materials. Renew. Energy 35 (6), 1319–1324.
Park, J.H., Ok, Y.S., Kim, S.H., et al., 2016. Competitive adsorption of heavy metals onto sesame straw biochar in aqueous solutions. Chemosphere 142, 77–83.
Peng, L.Z., Liu, L.L., Zhang, S.Q., et al., 2010. Heavy metals content in manure of commercial animal farms in Fujian Province. Journal of Fujian Agriculture and Forestry University (Natural Science Edition) 39 (5), 523–527.
Qin, J., Qian, S., Chen, Q., et al., 2019. Cow manure-derived biochar: its catalytic properties and influential factors. J. Hazard. Mater. 371, 381–388.
Shinogi, Y., Kanri, Y., 2003. Pyrolysis of plant, animal and human waste: physical and chemical characterization of the pyrolytic products. Bioresour. Technol. 90, 241–247.

Smith, K.M., Fowler, G.D., Pullket, S., et al., 2009. Sewage sludge-based adsorbents: a review of their production, properties and use in water treatment applications. Water Res. 43 (10), 2569–2594.
Sun, Y., Shah, K.J., Sun, W., Zheng, H., 2019. Performance evaluation of chitosan-based flocculants with good pH resistance and high heavy metals removal capacity. Sep. Purif. Technol. 215, 208–216.
Suthar, S., 2009. Vermicomposting of vegetable-market solid waste using *Eisenia fetida:* impact of bulking material on earthworm growth and decomposition rate. Ecologi. Engin. 35 (5), 914–920.
Tsai, W.T., Hsu, C.H., Lin, Y.Q., 2019. Highly porous and nutrients-rich biochar derived from dairy cattle manure and its potential for removal of cationic compound from water. Agriculture 9 (6), 114.
Wang, M., Li, S.T., 2014. Heavy metals in fertilizers and effect of the fertilization on heavy metal accumulation in soils and crops. J Plant Nut Fertil 20 (2), 466–480.
Wang, Z.Y., Zheng, H., Luo, Y., 2013. Characterization and influence of biochars on nitrous oxide emission from agricultural soil. Environ. Pollu. 174, 289–296.
Wang, H.Y., Gao, B., Wang, S.S., 2015a. Removal of Pb(II), Cu(II), and Cd(II) from aqueous solutions by biochar derived from $KMnO_4$ treated hickory wood. Bioresour. Technol. 197, 356–362.
Wang, Z.Y., et al., 2015b. Investigating the mechanisms of biochar's removal of lead from solution. Bioresour. Technol. 177, 308–317.
Wang, X., Li, X., Liu, G., et al., 2019. Mixed heavy metal removal from wastewater by using discarded mushroom-stick biochar: adsorption properties and mechanisms. Environmental Science: Processes & Impacts 21 (3), 584–592.
Wei, J., Tu, C., Yuan, G., Liu, Y., Bi, D., Xiao, L., Zhang, X., 2019. Assessing the effect of pyrolysis temperature on the molecular properties and copper sorption capacity of a halophyte biochar. Environ. Pollut. 251, 56–65.
Wnetrzak, R., Leahy, J.J., Chojnacka, K.W., et al., 2014. Influence of pig manure biochar mineral content on Cr (III) sorption capacity. J. Chem. Technol. Biotechnol. 89 (4), 569–578.
Wu, D., Wang, Y., Li, Y., et al., 2019. Phosphorylated chitosan/$CoFe_2O_4$ composite for the efficient removal of Pb (II) and Cd (II) from aqueous solution: adsorption performance and mechanism studies[J]. J. Mol. Liq. 277, 181–188.
Xu, X.Y., Cao, X.D., Zhao, L., 2013a. Removal of Cu, Zn, and Cd from aqueous solutions by the dairy manure-derived biochar. Environ. Sci. Pollut. Res. 20, 358–368.
Xu, X.Y., Cao, X.D., Zhao, L., 2013b. Comparison of rice husk and dairy manure-derived biochars for simultaneously removing heavy metals from aqueous solutions: role of mineral components in biochars. Chemosphere 92, 955–961.
Xue, Y., Wang, C., Hu, Z., et al., 2019. Pyrolysis of sewage sludge by electromagnetic induction: biochar properties and application in adsorption removal of Pb (II), Cd (II) from aqueous solution. Waste Manag. 89, 48–56.
Yang, X., Wan, Y., Zheng, Y., He, F., Yu, Z., Huang, J., Gao, B., 2019. Surface functional groups of carbon-based adsorbents and their roles in the removal of heavy metals from aqueous solutions: a critical review. Chem. Eng. J. 366, 608–621.
Yang, G., Wang, Z., Xian, Q., et al., 2015. Effects of pyrolysis temperature on the physicochemical properties of biochar derived from vermicompost and its potential use as an environmental amendment. RSC Adv. 5 (50), 40117–40125.
Yang, X., Lu, K.P., Kim, M.G., Chen, L., Hu, G.T., Wang, Q.Y., Liu, X.Y., Shen, L.L., Huang, H.G., Ye, Z.Q., Wang, H.L., 2017. Bioavailability of Cd and Zn in soils treated with biochars derived from tobacco stalk and dead pigs. J. Soils Sediments 17 (3), 751–762.
Yang, L., Wen, T., Wang, L., et al., 2019b. The stability of the compounds formed in the process of removal Pb (II), Cu (II) and Cd (II) by steelmaking slag in an acidic aqueous solution. J. Environ. Manag. 231, 41–48.
Yao, W., Zhu, W.Q., Zhan, Y.N., 2014. Adsorption of Cu(II) and Zn(II) ions by solidified landfilled sludge and its pyrolyzed produce. Advanced Materi. Resear. 955-959, 2629–2634.
Yin, D.X., Wang, X., Chen, C., Peng, B., Tan, C.Y., Li, H.L., 2016. Varying effect of biochar on Cd, Pb and As mobility in a multi-metal contaminated paddy soil. Chemosphere 152, 196–206.
Yu, J., Zheng, J., Lu, Q., et al., 2016. Selective adsorption and reusability behavior for Pb^{2+} and Cd^{2+} on chitosan/poly (ethylene glycol)/poly (acrylic acid) adsorbent prepared by glow-discharge electrolysis plasma. Colloid Polym. Sci. 294 (10), 1585–1598.
Yu, S., Liu, Y., Ai, Y., Wang, X., Zhang, R., Chen, Z., Wang, X., 2018. Rational design of carbonaceous nanofiber/Ni-Al layered double hydroxide nanocomposites for high-efficiency removal of heavy metals from aqueous solutions. Environ. Pollut. 242, 1–11.
Yuan, J.H., Xu, R.K., Zhang, H., 2011. The forms of alkalis in the biochar produced from crop residues at different temperatures. Bioresour. Technol. 102 (3), 3488–3497.
Zhang, X.H., 2016. Analysis on the development of industrial production of organic fertilizer. Agriculture and Technology 36 (2), 2.
Zhang, Z.D., Wu, J.G., 2010. Progress of the researches on resource utilization of livestock and poultry manure. Guangdong Agri. Sci. 1, 135–138.
Zhang, T., Bu, M., Geng, W., 2012. Pollution status and biogas-producing potential of livestock and poultry excrements in China. Chinese Journal of Ecology 31 (5), 1241–1249.
Zhang, Z.H., Yuan, Q.X., Dai, P., 2019. Biochar fertilizer utilization characteristics of mixed pyrolysis of livestock manure and straw. College of Engineering. Huazhong Agricultural University. Sci. 38 (1), 133–138.
Zhao, B., Oconnor, D., Zhang, J.L., Peng, T.Y., Shen, Z.T., Tsang, D.C.W., Hou, D., 2018. Effect of pyrolysis temperature, heating rate, and residence time on rapeseed stem derived biochar. J. Clean. 174, 977–987.
Zhu, W.Q., Jia, X.Y., Li, X.M., Cheng, H.X., 2008. Adsorption behaviour of cadmium and lead in pig manure waste and its vermicompost. J. Agro-Environ. Sci. 27 (5), 1796–1802.
Zhu, W.Q., Jia, X.Y., Li, X.M., 2009. Adsorption behaviour of copper and zinc on pig manure and its vermicompost. J. Agro-Environ. Sci. 28 (2), 180–186.
Zhu, W.Q., Zhi, Z., Jianli, S., 2012. Romoval of zinc ion from aqueous solution by adsorption on solidifying landfilled sludge. Adv. Mater. Res. 343-344, 62–66.
Zhu, W.Q., Yao, W., Shen, X.Y., Zhang, W.W., Xu, H.T., 2018. Heavy metal and δ 13C value variations and characterization of dissolved organic matter (DOM) during vermicomposting of pig manure amended with 13C-labeled rice straw. Environmental Science and Pollution Research 25, 20169–20178.
Zhu, X., Wang, X., Ok, Y.S., 2019. The application of machine learning methods for prediction of metal sorption on biochars. J. Hazard. Mater. 378, 120–127.